Renewable and Sustainable Energy Reviews 187 (2023) 113725

Contents lists available at ScienceDirect

Renewable and Sustainable Energy Reviews

journal homepage: www.elsevier.com/locate/rser

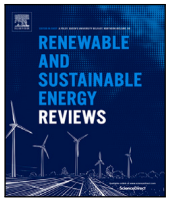

Performance analysis of a multi-source renewable energy system for temperature control in buildings of varied thermal transmittance and climate zone

Marco Cavazzuti *, Michele Bottarelli

Dipartimento di Architettura, Università degli Studi di Ferrara, via Ghiara 32, Ferrara, 44121, Italy

ARTICLE INFO

Keywords:
HVAC
PVT collector
Shallow ground geothermal energy
Phase change material
Radiant floor
Renewable energy system
System control

ABSTRACT

The current paper presents a numerical analysis of a multi-source renewable energy system for building air conditioning aiming at decarbonising the building envelope. The thermal management of the building is pursued through a radiant floor fed by a heat pump and integrated with phase change materials for thermal inertia enhancement. A fan coil is foreseen for humidity control. The heat pump can be fed through three parallel circuits involving different thermal sources: air with an ordinary air-to-water heat exchanger, sun through photovoltaic thermal solar collectors, and ground using shallow ground flat-panel heat exchangers. At need, the ground can be exploited for thermal energy storage when the heat pump is idle. A set of dedicated control rules chooses the optimal source or mix of sources to exploit at any time. Simulations of a reference building, namely a large single-room snack bar, are performed for various plant configurations, hypothesising the building as located in distinct climate zones and characterised by different thermal transmittance. The thermal performance of the building is given in terms of primary energy needs per year and compared to that of an analogous single-source plant. Results show that the proposed system can lead to primary energy savings of up to 16% compared to the corresponding state-of-the-art single-source plant, being more effective if the geothermal field is large enough and the building heating and cooling needs are comparable. The relevance of a proper control algorithm for plant performance optimisation is highlighted: a thermal power-based approach is proposed and successfully tested.

1. Introduction

Buildings play a considerable role in the global energy balance. According to Pérez-Lombard et al. [1] the global contribution given by residential and commercial buildings in terms of primary energy consumption is growing steadily due to the growth in population and the increasing demand for building services and has reached a share between 20% and 40% in developed countries, overcoming other major sectors such as industry and transportation. About half this energy is to be attributed to heating, ventilation, and air-conditioning so that the adoption of more efficient thermal management systems in buildings, together with a possibly wider deployment of renewable energy sources, becomes particularly relevant to limit world energy use and greenhouse gas emissions. To be noted that the exploitation of renewable sources also poses the issue of energy storage [2], needed to decouple thermal and electrical energy production from consumption. The literature on the topic is very large ranging from systems able to efficiently integrate and exploit different renewable energy sources, to ways for increasing the performance of a given source, or methods for storing the thermal energy at need.

Among the possible thermal sources, particular attention has been devoted to solar energy. One of the main drawbacks of photovoltaic panels is the low sunlight-to-electrical energy conversion rate of the solar cells. A large share of research has thus focused on means for improving the cells' efficiency or increasing the amount of solar energy absorbed. Among these are found perovskite cells [3,4], quantum dot cells [5,6], luminescent solar concentrators [7], luminescent down-shifting dyes able to reduce the solar radiation wavelength to ranges where solar cells work best [8,9], and compound parabolic concentrators [10,11].

A renovate interest is met also towards shallow ground geothermal applications for its lesser plant installation costs, reasonable efficiency, and no long-term ground thermal imbalance [12]. Among possible applications, ground heat exchangers in the form of pipes buried in boreholes [13] or also flat-panels in trenches [14,15], for an extended

* Corresponding author.
E-mail addresses: marco.cavazzuti@unife.it (M. Cavazzuti), michele.bottarelli@unife.it (M. Bottarelli).

https://doi.org/10.1016/j.rser.2023.113725
Received 23 May 2023; Received in revised form 29 August 2023; Accepted 6 September 2023
Available online 19 September 2023

Nomenclature

c	Specific heat
f	Weighting factor
F	Penalty function
$\dot{m}$	Mass flow rate
Q	Thermal energy
RH	Relative humidity
s	Season indicator
T	Temperature
U	Thermal transmittance

Greek symbols

Δ	Difference
ε	Heat exchanger efficiency
η	Efficiency

Subscripts

bld	Building
cl	Cooling
el	Electric
ht	Heating
in	Inlet
out	Outlet
pri	Primary state
rec	Receiver
sec	Secondary state
src	Source
sup	Supplier

Acronyms and abbreviations

A	Air source
AHU	Air handling unit
AHX	Air heat exchanger
BF	Buffer tank
CC	Current configuration
COP	Coefficient of performance
DHC	Direct heating/cooling
ETP	Expected thermal power
FC	Fan coil
G	Ground source
GHX	Ground heat exchanger
HP	Heat pump
M	Mixing device
MS	Multi-source
P	Pump
PC	Planned configuration
PCM	Phase change material
PVC	Photovoltaic cooling
PVT	Photovoltaic/thermal hybrid solar collector
RES	Renewable energy system
RF	Radiant floor
S	Sun source
SS	Single-source
UTES	Underground thermal energy storage
V	Valve
XC	Extended configuration

heat transfer area, are found. The techno-economic analysis in [16] estimates electric energy savings of up to 30% with the use of borehole ground heat exchangers in conjunction with heat pumps in place of common air heat exchangers. A recent review of the performance of ground heat exchangers can be found in [17]. In [18] the potential for carbon dioxide emission mitigation in urban areas of such systems is investigated, highlighting how they are particularly appropriate for low energy demand buildings, possibly located outside the city centre where the urban pattern is less dense and digging for the installation easier. In [19,20] the focus is on the European Union's legal framework concerning geothermal energy. It is stressed how the exploitation of shallow geothermal energy could benefit from common guidelines.

For what concerns multi-source renewable energy systems (RESs) the range of solutions is very large depending on the type of sources exploited and the way these are integrated into the system. For instance, in [21] a system integrating an organic Rankine cycle fuelled by biodiesel, a wind turbine, and a photovoltaic unit is proposed. In a similar fashion, in [22] a biomass boiler is put in parallel with solar thermal collectors feeding a heat pump, while in [23] a multi-source system for residential use is proposed where photovoltaic thermal hybrid solar collectors and borehole ground heat exchangers feed a water-to-water heat pump, in parallel to an air-to-water heat pump. Also, hydrogen-based applications for energy storage are investigated in conjunction with renewable energy production systems based on photovoltaic and wind [24,25]. The environmental impact of renewable energy systems is reviewed in [26] focusing on some of the most common technologies such as wind, hydroelectric, biomass, and geothermal.

A more systematic approach to the multi-source energy system design is also found in the literature, either for the optimal choice of the sources to be combined using multi-criteria decision-making algorithms [27] or in the sizing of the system components through multi-objective optimisation algorithms [28]. In [29,30] reviews on possible ways to model and design such multi-faceted and elaborated systems are given.

The work in [31] reviews the use of the ground source within multi-source energy systems, pointing out how its integration with the solar source is often proposed in the literature, even though the systems are rarely designed for electrical power generation through photovoltaic thermal hybrid solar collectors. It is also noted how the complexity of the control system remains the main obstacle to the correct exploitation of hybrid multi-source energy systems. The problem of optimal control is discussed in [32] where a solution addressing some control parameters is obtained using mixed-integer linear programming optimisation methods. Also, solutions based on fuzzy logic have been proposed and are reviewed in [33]. Nevertheless, the literature on the topic is kind of sparse.

Thermal energy storage is a key aspect of renewable energy systems. Thermal storage can be obtained in terms of sensible heat (*e.g.* heating or cooling a fluid tank), latent heat (through phase change materials), or thermo-chemical processes [34]. The use of phase change materials (PCMs) in RESs and buildings is still at a demonstration stage, although quite promising. Specialised literature often deals with the testing of different PCMs to enhance the thermal capacity of the storage, such as in [35] where a series of materials of different types, melting points, and latent heats are investigated in view of their application to buildings. Another major issue regards possible means to enhance the usually low thermal conductivity of PCMs, thus achieving larger thermal power rates. This is often pursued by metal fin [36], foam structures [37], or by blending with powder of some high thermal conductivity material such as graphene [38]. More common PCM applications in buildings regard components subject to temperature oscillations over relatively short periods of time that can benefit from mitigated temperature variations, such as water buffer tanks [39], radiant floors [40], building walls [41], roofs [42], construction bricks [43], solar collectors [44], or photovoltaic systems [45,46]. Application to components whose thermal inertia is large and whose temperature oscillation occurs too slowly, *e.g.* on a yearly basis as in the case of shallow ground [47], in general, is less viable as too large a thermal storage enhancement would be needed for its effect to be meaningful. Large reviews on the

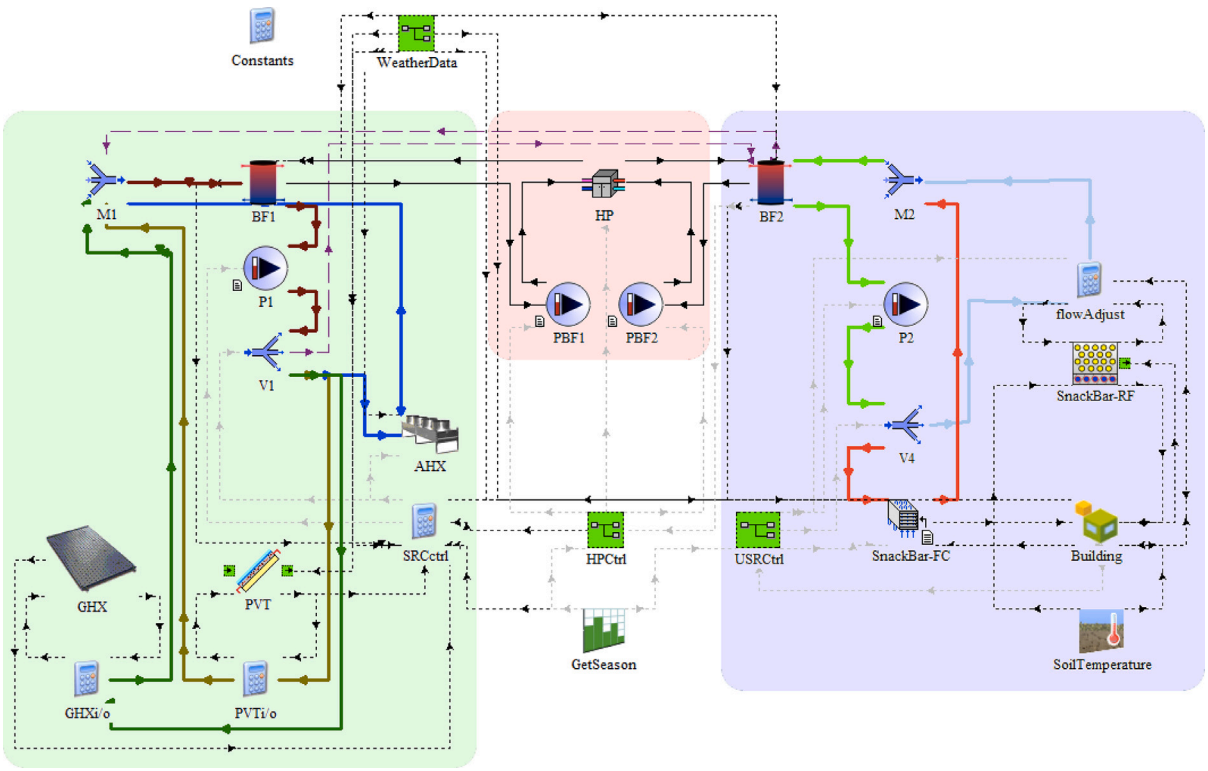

Fig. 1. The TRNSYS model layout. The model is composed of two parts, the sources side on the left, and the building side on the right, linked through the heat pump in the centre.

use of PCMs for thermal energy storage purposes are given in [48,49], and [50].

In the present paper, a novel integrated multi-source RES model for building air conditioning aiming at achieving cost-effective heating and cooling is presented and numerically investigated in TRNSYS, a transient simulation tool particularly suitable for systems composed of several components like the one at stake. The software also features a large library of common and less common component types fitting well the modelling needs encountered. The main goal of the study is to numerically assess the system performance on buildings of different thermal transmittances located in different climate zones. The system proposed is based on a heat pump exploiting air, sun, and ground as thermal sources through suitable heat exchangers. The thermal management of the building is achieved through a PCM-integrated radiant floor supported by fan coils at need. A novel system control algorithm, based on the prediction of the thermal power that could be exchanged by the system under different temperature and flow rate operating conditions, is discussed and successfully tested. The reference building over which the RES is evaluated consists of a large single-room snack bar located on the campus of the University of Ferrara where the proposed system is being installed and is going to be monitored in the near future for research purposes. The performance of the system is given in terms of primary energy savings that can be achieved compared to a more common air-based single-source similar plant and is evaluated under different scenarios in terms of plant configuration, climatic conditions, and building thermal transmittance. In this way, the relevance of the solution proposed can be assessed for various practical situations. Results show that primary energy savings in the range between 8% and 16% can be obtained, where best performances are met for climate areas where there is a net separation between a heating season (winter) and a cooling season (summer) that allows to periodically recharge the ground source thanks to its alternate use. The crucial role of a suitable control algorithm is also highlighted. The thermal power-based method proposed has been demonstrated to allow the buffer tank on the sources side to be thermally recharged quickly so that when the heat pump is turned on its temperature drift is limited and the heat pump coefficient of performance is preserved. This is particularly relevant considering the relatively small size of the buffer tank employed for feeding the heat pump. The work is part of the "novel building integration designs for increased efficiencies in advanced climatically tunable renewable energy systems" (IDEAS) project funded by the European Union under the Horizon 2020 framework programme.

2. Methodology

In this section the RES numerical model is presented. The building model is introduced at first, together with the different plant configurations analysed. The system operation modes and controls are discussed next, followed by the set of the simulations performed.

A generic view of the layout of the TRNSYS model in its most general form is shown in Fig. 1 for reference.

2.1. The building

The reference building used to test the RES is the snack bar of the biomedical centre of the University of Ferrara shown in Fig. 2. Energy requalification works of the building are currently ongoing in line with the IDEAS project provisions, whereas the proposed RES has already been installed on a small scale test facility at the TekneHub laboratory of the University of Ferrara, which is part of the High Technology Network of laboratories for research and innovation of the Emilia-Romagna region in Italy.

The building has a floor surface of 134 m^2 subdivided into two areas: the bar counter (34 m^2) and the rest of the room (100 m^2). Following the requalification works, on the latter a PCM integrated radiant floor is going to be installed, while on the former the previous regular floor will remain. The height of the flat ceiling is 3.15 m for an overall room volume of 422 m^3. The building footprint is 12 m in the east–west, and 12.8 m in the north–south directions. Lateral walls and ceiling area

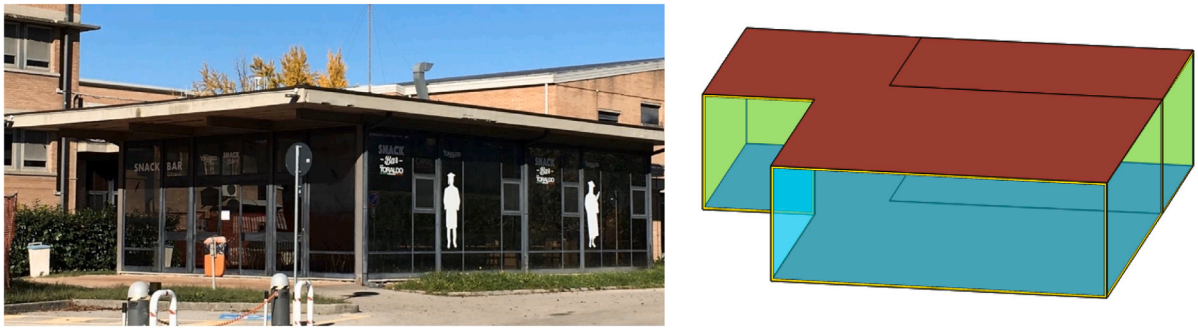

(a) External view of the snack bar from south-east (b) TRNBuild model of the snack bar

Fig. 2. The reference building.

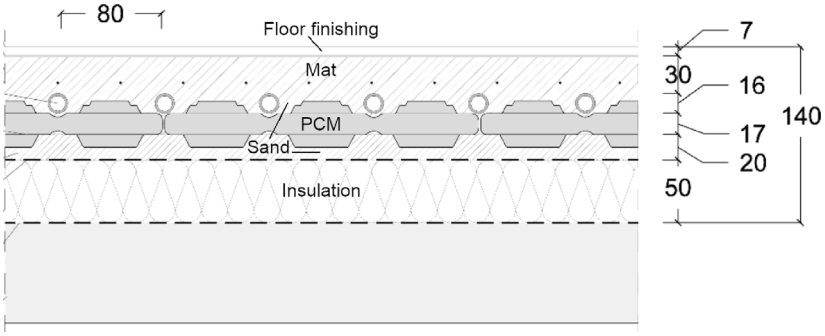

Fig. 3. The radiant floor layering, dimensions are in mm.

amounts to 290 m^2, 93 m^2 of which are glazed windows with iron frame facing mostly south and east, the rest being made of bricks.

The walls and the regular floor are modelled as generic single layer walls of given thermal transmittance U. The thermal transmittance of the walls can be varied between 0.25 W/m^2K and 0.70 W/m^2K in order to evaluate buildings of different thermal performance. The thermal transmittance of the regular floor, instead, is kept fixed at 0.25 W/m^2K, *e.g.*

$$U = \left(\frac{1}{h_i} + \frac{t}{\lambda} + \frac{1}{h_o}\right)^{-1} = \left(\frac{1}{7.7} + \frac{0.3}{0.0783} + \frac{1}{25}\right)^{-1} \frac{W}{m^2K} = 0.25 \frac{W}{m^2K} \quad (1)$$

where the choice of the convective coefficients follows UNI EN 6946 standard. Thermal absorptance and emissivity of the wall surfaces are set to 0.9. Windows are modelled as double glazed having U=1.1 W/m^2K, g=0.62, and featuring no inner shading devices. External solar radiation shading on walls and windows is due to both the neighbouring buildings and the cantilevered roof of the snack bar as shown in Fig. 2(a). In the building model, constant shading factors averaging the real situation are applied as follows: 100% shading on the brick walls facing north and west, 50%, 35%, and 10% shading for the glazed windows facing west, south, and east, respectively.

Air change rate due to infiltrations from the ambient is set to 0.2 volumes per hour.

For what concerns the radiant floor, the outer diameter of the floor pipes is 16 mm, including a wall thickness of 2 mm with thermal conductivity λ=0.35 W/mK. The spacing between the pipe rows is 80 mm, for an overall pipes length of 1250 m. From top to bottom, the radiant floor layering is shown in Fig. 3.

Below the floor finishing (t=7 mm, λ=0.35 W/mK) is a mat (t=30 mm, λ=1.2 W/mK). Beneath the mat, the pipes are immersed in sand (t=16 mm, λ=1.2 W/mK), laid above flat PCM containers (t=13 mm, λ=0.485 W/mK) with plastic walls on each side (t=2 mm, λ=0.44 W/mK), and an additional sand layer (t=20 mm, λ=1.2 W/mK). An insulation panel (t=50 mm, λ=0.04 W/mK) is placed at the bottom, over the existing substratum. Each PCM container has an area of 0.125 m^2, resulting in 800 containers being laid overall, equally subdivided between two types of salt hydrate PCMs to enhance the floor thermal inertia both in heating and cooling operating conditions: the first with nominal melting point at 27 °C and total latent heat of 18 MJ, the other with nominal melting point at 17 °C and total latent heat of 15 MJ. Water mass flow rate is set to 1500 kg/h when the radiant floor is in operation.

The radiant floor is backed at need for heating, cooling, and humidity control purposes by an air-to-water fan coil. Air flow rate is fixed by the required air exchange rate set to 10 volumes per hour (*i.e.* 4220 m^3/h) according to UNI 10 339 italian standard with a 75% efficiency heat recovery system, while water flow rate is set to 4500 kg/h when in operation. No inner air recirculation is foreseen as suggested by recent rules for SARS-CoV-2 prevention in indoor public environments. The nominal total heating and cooling powers of the fan coil are set to 13.25 kW, the nominal sensible cooling power to 9 kW, whereas the nominal fan electric consumption is 450 W. The fan coil model is based on normalised lookup tables giving the total and sensible heat transfer rates for different operating conditions in terms of air and water mass flow rates, inlet water temperature, and inlet dry and wet bulb temperatures of the air. The lookup tables were created from detailed data on a commercial fan coil similar to the one installed in the building.

The radiant floor and, depending on the plant configuration as will be discussed next, the fan coil are fed by a 2 m^3 water buffer tank insulated with a layer of 10 cm of high-density polyethylene for a heat loss rate to the ambient of 2.4 W/K.

A variable speed pump having nominal mass flow rate of 9000 kg/h and nominal electric consumption of 600 W circulates the water between the buffer tank, the radiant floor ($\dot{m}$=1500 kg/h), and the fan coil ($\dot{m}$=4500 kg/h) at need. The pump electric consumption $\dot{P}$ is assumed to vary with the mass flow rate $\dot{m}$ according to

$$\dot{P} = \dot{P}_{nom}\left[0.25 + 0.25\left(\frac{\dot{m}}{\dot{m}_{nom}}\right) + 0.50\left(\frac{\dot{m}}{\dot{m}_{nom}}\right)^2\right]. \quad (2)$$

Eq. (2) interpolates data from the technical sheet of the pump to be installed in the real plant.

Boundary conditions for the building are the ambient conditions taken from weather files of the specified location given in TMY2 format for walls and ceiling, and the undisturbed soil temperature function at 1 m depth for a soil having thermal diffusivity of 0.417 mm^2/s for the floor. The walls inner and outer convective heat transfer coefficients are set to h_i=7.7 W/m^2K and h_o=25 W/m^2K while the floor is linked to the soil temperature through an equivalent heat transfer coefficient h_o=0.5 W/m^2K.

The building is modelled in TRNSYS with Type 56 (multi-zone building), the radiant floor with Type 399 (phase change materials in passive and active wall constructions), the fan coils with Type 996 (performance map fan coil), the buffer tank with Type 534 (cylindrical storage tank with immersed heat exchangers), the pump with Type 110 (variable speed pump), and the soil temperature boundary condition with Type 77 (soil temperature profile).

The current analysis addresses only the heating and cooling needs of the building and the electrical consumptions directly associated to the air conditioning plant, and does not include the electric energy consumption nor the thermal gains due to the bar equipment, lighting, and people, nor the thermal needs associated to hot sanitary water.

2.2. The sources

On the sources side, the RES proposed consists of three parallel water loops feeding a buffer tank having the same capacity and characteristics of the tank on the building side. On each loop a different thermal source (namely, ground, air, and sun) is exploited through dedicated heat exchangers. A nominal water mass flow rate of 6000 kg/h is expected in the circuit under ordinary operating conditions.

Ground is exploited by means of flat-panels ground heat exchangers (GHXs) having external dimensions of 2 m×1 m×16 mm and, casing excluded, holding 16 litres of water each. The panels are installed vertically in the shallow ground at an average depth of 1.9 m. 8 series of 6 panels (*i.e.* 12 m long) are installed in parallel for a total of 48 panels and an active heat transfer area of 192 m^2. The geothermal lines are spaced between them so as not to thermally interfere with each other. The heat transfer efficiency of the lines has been estimated to be equal to 86% at the nominal water mass flow rate of 6000/8 kg/h=750 kg/h.

Air is exploited by means of a commercial air-to-water heat exchanger (AHX) characterised by a nominal air mass flow rate of 7000 kg/h and water mass flow rate of 6000 kg/h. Under these circumstances, when the temperature difference between the entering streams is 20 °C the thermal power exchanged is 20 kW, with a heat transfer efficiency of 51%. The nominal fan electric consumption amounts to 500 W.

Sun is exploited by means of photovoltaic thermal (PVT) hybrid solar collectors installed on the roof of the building and providing both electric and thermal energy. 10 solar panels are installed having a nominal peak electric power production of 400 W for an active surface area of 1.96 m^2 each. The panels are thermally connected in parallel. The PVT heat transfer efficiency has been estimated to be 46% at the nominal water mass flow rate of 6000/10 kg/h=600 kg/h.

A variable speed pump the same as the one on the building side circulates the water between the buffer tank and the source loops. A series of three way valves splits the flow among the sources as prescribed by the system control algorithm. For simplicity and with no loss of generality, it is assumed that for any total mass flow rate in the circuit, the pump electric consumption always follows Eq. (2). This means that the pressure drop is assumed to be the same whatever loop or group of loops are exploited at each time. A finer setup for the simulations could be easily implemented once the plant is built and the real pressure loss coefficients are known more in detail. The pump mass flow rate can vary between 4000 kg/h and 8000 kg/h and is governed by the control algorithm on the basis of the thermal load on the system.

In TRNSYS, the GHX is modelled with a in-house developed Type [51], the AHX with Type 511 (dry fluid cooler), and the PVT with Type 555 (PV-PCM Module) that can also model the use of PCM to increase the thermal inertia in the solar panel heat exchanger. This represents a possible extension to the proposed system currently being tested in the small scale laboratory facility.

2.3. The heat pump

A water-to-water heat pump operates between the two buffer tanks: the one on the sources side, and the one on the building side. Two recirculation pumps move the water from the tanks to the heat pump and back. When the heat pump is operating, the recirculation pumps work at a fixed point. The pump on the sources side delivers a mass flow rate of 5000 kg/h with an electric consumption 125 W, while for the pump on the building side $\dot{m}$=4000 kg/h and $\dot{P}$=100 W.

The nominal heating and cooling power of the heat pump is 26 kW with a nominal electric consumption of 7 kW, which corresponds to nominal coefficient of performance (COP) and energy efficiency ratio (EER) of 3.71. The heat pump model is based on normalised lookup tables giving the heat transfer rate and the electric consumption for different operating conditions in terms of water mass flow rate and inlet temperature at the heat pump condenser and evaporator. The lookup tables were created from detailed data on a commercial heat pump similar to the one that will be installed in the building.

The heat pump is modelled in TRNSYS with Type 927 (water-to-water heat pump), the recirculation pumps with Type 110 (variable speed pump).

2.4. The plant configurations

A total of 5 different heating and cooling system configurations are investigated and compared.

First, there is the current configuration (CC) which is not based on renewable energy. Currently, air conditioning in the snack bar is achieved through the heating and cooling plant of the university complex consisting in a large air handling unit (AHU). The treated air is introduced in the room through air diffusers located on the ceiling. From the modelling point of view the AHU is not addressed in detail as this would go beyond the scope of the current work: it is assumed that the university plant provides water at a fixed temperature to an air-to-water fan coil in the room, and that this hot/cold water is obtained from processes of given thermal performance typical of common condensing boilers and commercial air conditioners. The inlet water temperature depends on whether the system is working in heating or cooling mode, while the water mass flow rate is set to 6000 kg/h when the fan coil is on. This is the same flow rate foreseen for the plant proposed when both the radiant floor and the fan coil are turned in operation as discussed in Section 2.1. In this way, plants having similar characteristics are compared. The thermal energy transferred through the fan coil is then accounted for, providing a mean for evaluating the thermal energy needs of the building. A very simple scheme of the air conditioning plant of the CC is given in Fig. 4(a).

The second configuration addressed is the multi-source planned configuration (MS-PC) which is the one that is going to be installed in the snack bar in the near future. This configuration is more complex as it features the complete multi-source system described previously. On the building side, the water buffer tank only feeds the radiant floor. The current AHU, in fact, will remain in operation being handled in a different way: it will operate only for granting the required air change rate in the room, for humidity control, and for heating and cooling purposes in case the radiant floor alone is not able to maintain the desired setpoint temperature in the room. A simplified scheme of the air conditioning plant of the MS-PC is given in Fig. 4(b).

The third configuration is the multi-source extended configuration (MS-XC) and is very similar to the second, the only difference being

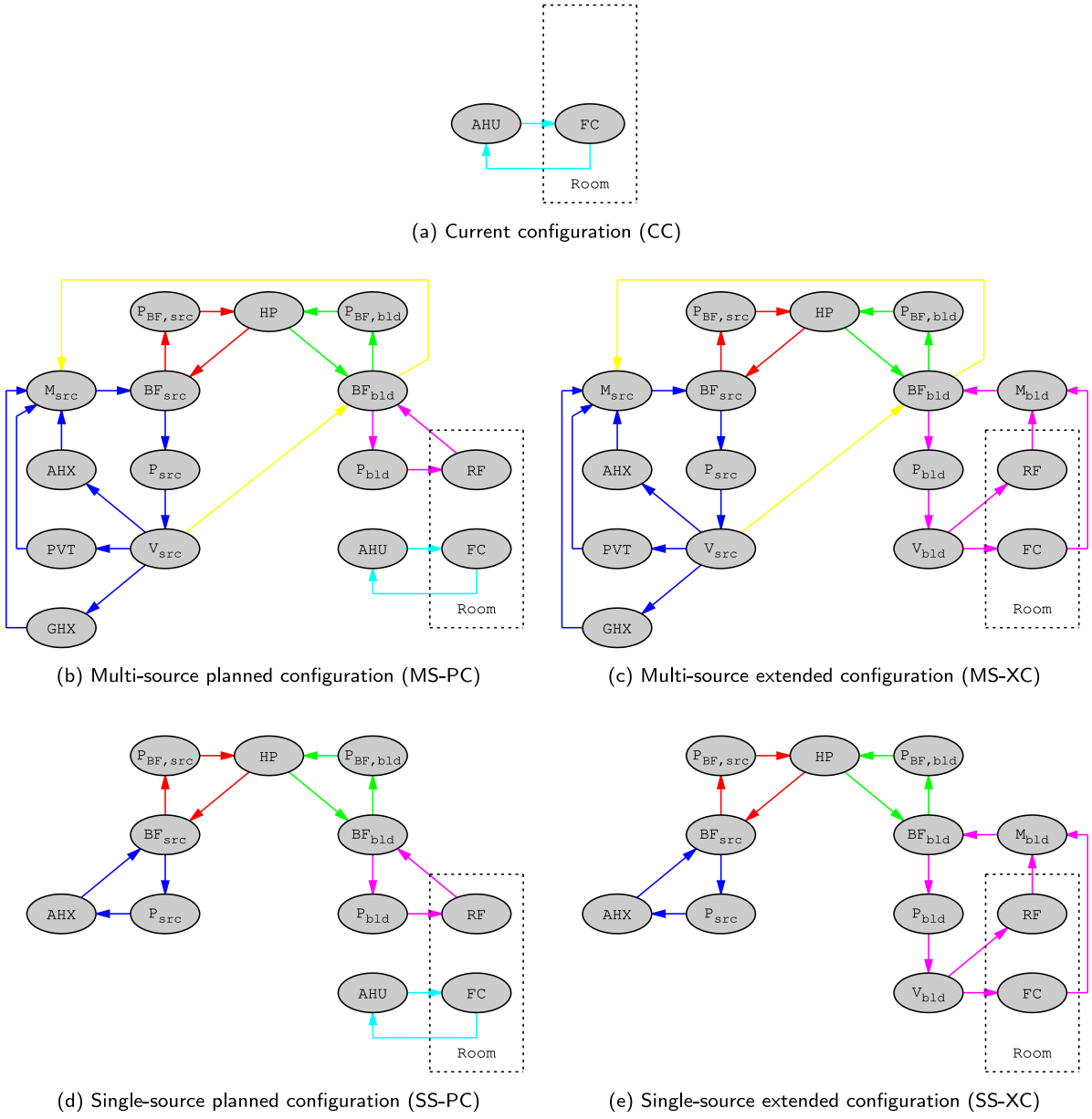

Fig. 4. Simplified schemes of the water loops in the different plant configurations. Symbols are as follows: heat pump (HP), pump (P), buffer tank (BF), radiant floor (RF), fan coil (FC), valve (V), mixing device (M). Subscripts "src" and "bld" denote the sources and the building sides respectively. The loops are highlighted as follows: sources side (blue), building side (magenta), BF to HP (red and green), AHU (cyan). An additional bypass loop between sources and building that will be discussed in the following is reported in yellow.

in the fact that the RES now feeds both the radiant floor and the fan coil on the building side. This configuration is the one that would be expected in case of installation in a new building where no previous air conditioning system is present, thus making the installation of an AHU unpractical. This configuration is also more demanding on the sources that now must cover the thermal needs of the building in full. A simplified scheme of the air conditioning plant of the MS-XC is given in Fig. 4(c), while the TRNSYS model layout is the one in Fig. 1.

Comparing the thermal performance of the multi-source configurations with the current would not hold a particular interest as the thermal systems are very different from each other, and the current configuration is not expected to be particularly performing. It is deemed more significant to compare the multi-source configurations with similar single-source systems where only air is used as a source, being air the most commonly exploited source in these kind of installations.

Thus, the fourth and the fifth configurations analysed are the air-based single source (SS) counterparts of the multi-source configurations above. In order to limit the changes and keep the models as similar and comparable as possible, the same water-to-water heat pump is assumed, the extra sources dropped, and the AHX loop kept. Even though an air-to-water heat pump would have been a preferable option, at least in a real plant, the reason for this choice is that the change of the heat pump and of the associated lookup tables would have been a major change in the system that would have made the different configurations less comparable. Simplified schemes of the single source air conditioning plants are given in Figs. 4(d) and 4(e).

The fluid employed in all the liquid loops in Fig. 4 is a mixture of 80% water and 20% propylene glycol with a density of $1015\,\mathrm{kg/m^3}$ and a specific heat of $3.99\,\mathrm{kJ/kg}$ at normal temperature and pressure conditions.

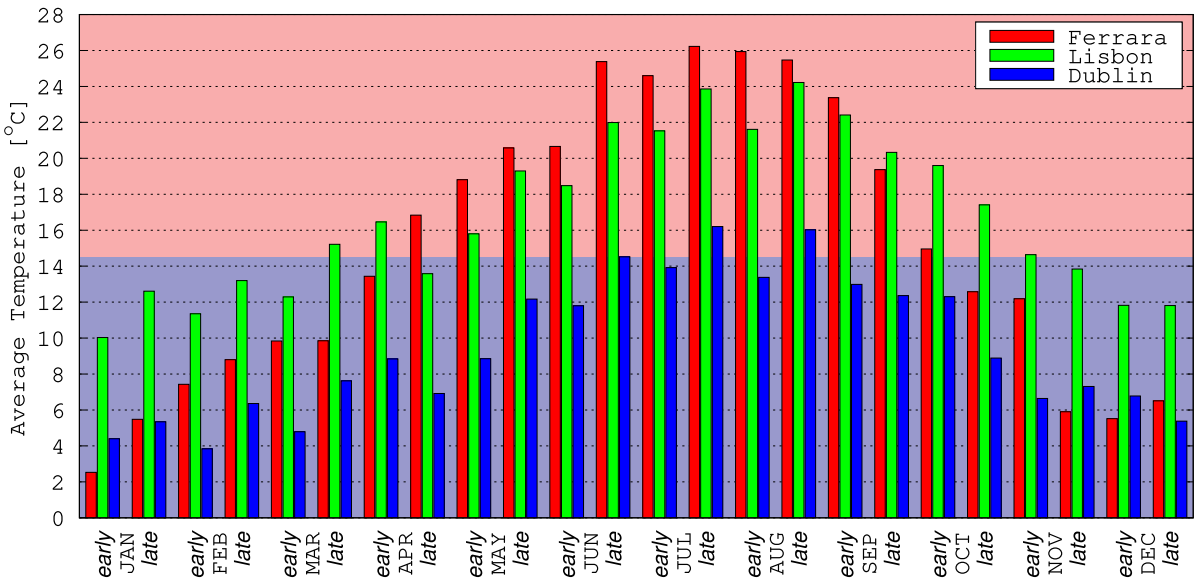

Fig. 5. Average daily temperature in Ferrara, Lisbon, and Dublin along the year.

Table 1
Target room temperature and relative humidity with deadbands, and heating and cooling periods.

	Heating season (winter)	Cooling season (summer)
Day (7AM–7PM)	T=21±0.5° C/RH=70±5 %	T=26±0.5° C/RH=70±5 %
Night (7PM–7AM)	T=17±0.5° C/RH=70±5 %	T=30±0.5° C/RH=70±5 %
Ferrara	Oct 16th–Apr 17th (6 months)	Apr 17th–Oct 16th (6 months)
Lisbon	Nov 16th–Mar 18th (4 months)	Mar 18th–Nov 16th (8 months)
Dublin	Jan 1st–Dec 31st (12 months)	– (0 months)

Table 2
Target building side buffer tank temperature.

Plant configuration	Heating season	Cooling season
Planned	37.5±1.5° C	12.5±1.5° C
Extended	41.5±1.5° C	9.5±1.5° C

2.5. The building control strategy

On the building side, the system control strategy aims at maintaining a given setpoint temperature and relative humidity in the air conditioned room. The target temperature varies with the time of the day and the season as in Table 1.

Working hours from 7AM to 7PM are assumed, while the year is split into a heating and a cooling season for what concerns the behaviour of the air conditioning plant. The subdivision of the year into these two periods of time depends on the geographic location. Three European climate areas are addressed, namely: Ferrara (Italy) having a continental climate with warm summers and cold winters, Lisbon (Portugal) having a mild mediterranean climate, and Dublin (Ireland) having a cold oceanic climate. Average temperatures over the year, where the year is split into 24 periods of 365 h each, are resumed in Fig. 5 for the three locations, from which the seasons subdivision in Table 1 is derived.

In TRNSYS numerical model, radiant floor and fan coil on/off signals are deduced from a set of differential controllers on the basis of the target values and the deadbands in Table 1: Type 970 and Type 971 (N-stage differential controller with time delays and multiple deadbands) for thermostats, and Type 2 (on/off differential controller) for humidity. Pumps and valves are then adjusted in order to deliver the required mass flow rate to the devices. Daily and seasonal temperature targets are set with on/off signals from Type 14 (time dependent forcing function).

With the exception of the current configuration where the radiant floor is missing, the room heating and cooling needs are preferably covered by the radiant floor. This behaviour is obtained by offsetting the fan coil on/off signal by 1 °C with respect to the values in Table 1. For instance, in a hot summer day the radiant floor will turn on when the room temperature exceeds 26.5 °C, while the fan coil will support the radiant floor being switched on once the room temperature grows beyond 27.5 °C. The fan coil will then turn off when a temperature lower than 26.5 °C is restored, and the radiant floor when T<25.5 °C. Of course, relative humidity is always controlled by the fan coil.

The AHU is assumed to deliver water at a constant temperature of 45 °C in heating mode, and of 7 °C in cooling mode.

2.6. The heat pump control strategy

The main scope of the heat pump is to keep the buffer tank on the building side (BF_{bld} in Fig. 4) at the desired temperature so that the system is always ready to answer to the thermal requests of the building. For this reason, the heat pump operation is governed by the temperature of this tank. The buffer tank target temperature depends on the season and the plant configuration and is set following Table 2.

The choice of different target temperatures for the different configurations is due to the fact that milder temperatures are in general advisable for feeding a radiant floor (as in the planned configuration), whereas this is not the case for fan coils. For this reason, intermediate temperatures between the planned configuration and the AHU inlet are chosen for the extended configuration where the same buffer tank must feed both the radiant floor and the fan coil. In the numerical model, the heat pump on/off signals are deduced once again from a set of differential controllers.

2.7. The system operation modes

The main goal of the sources control strategy is to keep the temperature of the buffer tank on the sources side (BF_{src} in Fig. 4) as close as possible to that of the buffer tank on the building side (BF_{bld}), compatibly with the available thermal sources. In this way, the thermal gap at the ends of the heat pump is reduced and its COP increased.

Table 3
Resume of the possible system states.

State	Type	Sources	Mass flow rate fraction to			
		Involved	GHX	AHX	PVT	BF_{bld}
Idle	–	None	–	–	–	–
G	Primary	GHX	1	0	0	0
A	Primary	AHX	0	1	0	0
S	Primary	PVT	0	0	1	0
GA	Primary	GHX+AHX	f_G	$1-f_G$	0	0
GS	Primary	GHX+PVT	f_G	0	$1-f_G$	0
GA UTES	Secondary	GHX+AHX	f_G	$1-f_G$	0	0
GS UTES	Secondary	GHX+PVT	f_G	0	$1-f_G$	0
AS PVC	Secondary	AHX+PVT	0	f_A	$1-f_A$	0
A DHC	Secondary	AHX	0	f_A	0	$1-f_A$
S DHC	Secondary	PVT	0	0	f_S	$1-f_S$

Air (A) through AHX and sun (S) through PVT are thermal sources whose temperature can change rather quickly over the day, and whose temperature does not depend on their degree of exploitation, if not marginally for sun, but on the meterological conditions. As such, they should be exploited by the system whenever deemed convenient.

Ground (G) instead, has a large thermal inertia and changes its temperature slowly, on a seasonal basis, being slightly out of phase compared to the average ambient temperature. This means that shallow ground would naturally remain relatively warm in winter time and cold in summer, thus representing an ideal thermal source for the building needs. On the other hand, local ground temperature does indeed depend on the degree of exploitation of the source, and an excessive exploitation could deplete the thermal source rather quickly making it unsuitable to be further exploited even for the rest of the season. Thus, attention should be paid in the control algorithm to preserve the ground source when possible.

The control strategy must then choose the most convenient thermal source, or mix of sources, to be exploited at any time to thermally recharge (*i.e.* heating or cooling depending on the season) BF_{src} at best. Besides, once the buffer tank is recharged, additional operations may be performed by the system in order to improve its energy efficiency such as, for instance, storing heat/cool in the ground through another source for later use.

Thus, a number of system states can be identified as in Table 3.

The table distinguishes between primary states whose goal is to recharge the buffer tank, and secondary states where additional operations are performed.

Among primary states there is the exploitation of a single source (G, A, or S), or also of two sources at a time (GA or GS). The rationale behind the latter is to limit ground exploitation by blending its use with another source when convenient.

Among secondary states, the system can perform underground thermal energy storage (UTES) by using ground in parallel to another source to thermally recharge the ground. For instance, this might be convenient during the heating season when heat is being drawn from the ground so that its temperature may fall below that of air. Another possible secondary operation is the photovoltaic cooling (PVC) that can be obtained by putting AHX and PVT in a loop in case the panels overheat during a hot summer day. Finally, direct heating/cooling (DHC) of the buffer tank on the building side can be performed bypassing the heat pump and putting air or sun sources directly in a parallel loop with BF_{bld} (see the yellow lines in Fig. 4). DHC is included among the possible system states even though it is actually rare that the temperature of the sources is such to make these states convenient, if not occasionally at the change of season.

In case BF_{src} does not need to be recharged, and no secondary state is energetically convenient, the pump on the sources side is momentarily switched off leaving the system idle.

2.8. The sources control strategy

The sources control strategy proposed is based on the assessment of the expected thermal power $\dot{Q}$ that can be drawn from the sources at each moment with each possible state. The rationale is that the best source to be exploited is the one that can transfer heat more rapidly so that the buffer tank on the sources side can maintain a more favourable temperature during the heat pump operation.

Let us focus for now on single-source primary system states. The thermal power transferred by the source to the water coming from BF_{src} can be written as

$$\dot{Q} = \dot{m}c\left(T_{out} - T_{in}\right) = \varepsilon_{src}\dot{m}c\left(T_{src} - T_{in}\right) \tag{3}$$

where $\dot{m}$ and c refer to water, in/out to the water inlet and outlet, and src to the source. With no loss of generality, the heat exchanger efficiency ε_{src} must here be intended "as seen by water", that is to say, under the hypothesis of infinite capacity of the outer mean. This, in first approximation, results in the efficiencies reported in Section 2.2 except for the AHX whose efficiency drops to 15%. Suitable reference temperature for the sources are those of the ambient for T_A, of the PVT cells for T_S, and of the outer surface of the flat-panel for T_G, whereas T_{in} is the temperature of the water in BF_{src}.

From Eq. (3), the water outlet temperature from the source heat exchanger can then be written as

$$T_{out} = \varepsilon_{src}T_{src} + \left(1 - \varepsilon_{src}\right)T_{in}\,. \tag{4}$$

Still from Eq. (3), by knowing the efficiency of the heat exchangers of each source, it is possible to predict the expected thermal power (ETP) that can be transferred in each state, being the temperatures and the mass flow rate in the system known at each time. Even though the efficiencies are expected to vary moderately with the mass flow rate, for simplicity they are here assumed constant and computed at the nominal mass flow rate as discussed in Section 2.2. It is also reminded that the mass flow rate for a given pump electric consumption is assumed to be the same whatever the source loop exploited. By dropping the constant terms $\dot{m}$ and c, it is practical to express the ETP index in °C as

$$ETP_{src} = s\varepsilon_{src}\left(T_{src} - T_{in}\right) = \frac{s\dot{Q}}{\dot{m}c} \tag{5}$$

where s is a season indicator whose value is +1 during the heating season and −1 during the cooling season. In this form, the higher the ETP the better the source. It is worth mentioning that with the nominal mass flow rate of 6000 kg/h given in Section 2.2 and the specific heat of 3.99 kJ/kg discussed in Section 2.4 an ETP=1 °C corresponds to a heat transfer rate $\dot{Q}$= ± 6.65 kW.

The extension of the analysis in order to account for mass flow rate dependent efficiencies, and different mass flow rates in each loop is trivial and can be obtained by substituting in Eq. (5)ε_{src} with a $\varepsilon_{src}(\dot{m}_{src})$ function, and including the $\dot{m}_{src}$ term as a function of the pump power for each source, possibly in a normalised form to keep the ETP index expressed in °C for convenience.

While air and sun should always be exploited if their ETP is positive and maximum, the same cannot be said for ground, as this source must be preserved from possible depletion. In case the best source occurs to be the ground, an estimate of the rate at which BF_{src} buffer tank is being discharged (ΔT_{max}) when the heat pump is working should be given. If air or sun can still satisfy such a demand they should rather be used in place of ground. Otherwise, if ground exceeds the thermal needs of the system, it should be blended in parallel with other sources so that the desired thermal power is delivered and the ground exploitation limited.

From preliminary simulations it was shown that with the simulated heat pump the peak thermal load on BF_{src} occurs in the cooling season and equals 40 kW. This means that a source having an ETP=6.0 °C can recharge the buffer tank fast enough to maintain the buffer tank temperature when the heat pump is working under the worst thermal load scenario. Thus ΔT_{max}=6.0 °C is chosen, even though other choices

are viable. When the heat pump is off, instead, BF_{src} may still need to be recharged even though a fast recharging is no longer a priority. A minimum allowable recharge rate (ΔT_{min}) is set to prevent the pump from working when too little heat would be transferred to/from the buffer tank. Preliminary simulations suggest that the best system performance is obtained for ΔT_{min}=3.0 °C.

If the heat pump is off and no source can recharge the buffer tank at the minimum target rate, then secondary system states can be selected. Secondary states always involve two sources in parallel to each other (or a source and the buffer tank BF_{bld} in case of DHC) both linked to BF_{src}: one supplying heat/cool, and the other receiving heat/cool and thus working in inverse mode. The necessary condition for a secondary state to be meaningful, beyond it being a mere discharge of BF_{src} to the receiver, is that the thermal gradient between the two sources is in the desired direction, *i.e.* $s(T_{sup}-T_{rec})>0$.

A suitable parameter to quantify the ETP index associated to secondary states could be something like the difference of the heat transferred by the two sources involved, weighted over the mass flow rate fraction crossing each source

$$ETP_{sec} = f_{sup} ETP_{sup} - f_{rec} ETP_{rec} . \tag{6}$$

where $f_{sup}+f_{rec}=1$, and $f \in (0, 1)$. Such an equation, even though it gives a correct picture of the instantaneous heat transfer, it has the disadvantage of depending on the temperature of BF_{src}, which is likely to change quite rapidly once the state is activated. A more representative evaluation of the potential of a secondary state should rather depend only on the temperature difference between the two sources involved. The optimal working point for a secondary state would be one which is stable, and whose *ETP* is maximum. By stable it is meant that the thermal power supplied by one source equals the amount received by the other so that BFsrc is subject to no thermal drift. Mathematically, this can be written as

$$f_{sup} ETP_{sup} = -f_{rec} ETP_{rec} \quad \Rightarrow \quad f_{sup} = \frac{ETP_{rec}}{ETP_{rec} - ETP_{sup}} \quad ;$$
$$f_{rec} = \frac{ETP_{sup}}{ETP_{sup} - ETP_{rec}} . \tag{7}$$

Substituting Eq. (7) into Eq. (6)

$$ETP_{sec} = \frac{2 ETP_{rec} ETP_{sup}}{ETP_{rec} - ETP_{sup}} = \frac{2 s \varepsilon_{rec} \varepsilon_{sup} \left(T_{rec} - T_{BFsrc}\right) \left(T_{sup} - T_{BFsrc}\right)}{\varepsilon_{rec} \left(T_{rec} - T_{BFsrc}\right) - \varepsilon_{sup} \left(T_{sup} - T_{BFsrc}\right)} \tag{8}$$

it is found. For given source temperatures and heat transfer efficiencies, assuming T_{BFsrc} as a variable, the optimal buffer tank temperature that maximises ETP_{sec} can be found by posing

$$\frac{\partial ETP_{sec}}{\partial T_{BFsrc}} = 0 \tag{9}$$

which, after a few algebraic passages, results in

$$T_{BFsrc} = T_{sup} - \left(T_{sup} - T_{rec}\right) f_{sup} = T_{rec} + \left(T_{sup} - T_{rec}\right) f_{rec} \tag{10}$$

where

$$f_{sup} = \frac{1 - \sqrt{\frac{\varepsilon_{sup}}{\varepsilon_{rec}}}}{1 - \frac{\varepsilon_{sup}}{\varepsilon_{rec}}} \quad ; \quad f_{rec} = \frac{1 - \sqrt{\frac{\varepsilon_{rec}}{\varepsilon_{sup}}}}{1 - \frac{\varepsilon_{rec}}{\varepsilon_{sup}}} = 1 - f_{sup} \tag{11}$$

and from which the corresponding *ETP* is found to be

$$ETP_{sec} = 2 s \varepsilon_{sup} f_{sup}^2 \left(T_{sup} - T_{rec}\right) = 2 s \varepsilon_{rec} f_{rec}^2 \left(T_{sup} - T_{rec}\right) . \tag{12}$$

Eq. (12) does not depend on the temperature of BF_{src}, and gives the ETP index of the optimal stable working condition towards which the secondary state naturally tends during its operation if the mass flow rate fraction is chosen following in Eq. (11). In fact, in case T_{BFsrc} is at first closer to T_{sup}, then the first term on the right-hand side of Eq. (6) will be smaller than the second in modulus. This will drive the temperature of the buffer tank towards T_{rec}. An equilibrium is found when Eq. (10) is met.

Table 4
Resume of the system secondary states with their multiplication factors.

Secondary state	Heat/Cool supplier	Heat/Cool receiver	Multiplication factor
GA UTES	AHX	GHX	$0.72F$
GS UTES	PVT	GHX	$2F$
AS PVC (cool only)	AHX	PVT	(T_{PVT}>50° C)
A DHC	AHX	BF_{bld}	0.36
S DHC	PVT	BF_{bld}	1

Storing a certain amount of thermal power in the ground (UTES) by means of AHX may not have the same beneficial overall effect on the system and the same cost in terms of electricity as, for instance, transferring the same thermal power to the buffer tank on the building side (DHC) by means of PVT. For this reason, the *ETP* in Eq. (12) is multiplied in practice by a non-negative coefficient derived from calibration on the basis of preliminary simulation. Table 4 resumes all the possible secondary states, together with their associated multiplication factor. For what concerns DHC states, their *ETP* can still be computed from Eqs. (11) and (12) by assimilating the buffer tank to a heat exchanger with ε=1 (direct mixing) and T_{src} equal to the temperature of the fluid in the tank.

With reference to Table 4, is to be noted that, unlike other states, PVT cooling is never operated to improve the overall energy performance of the system but only to protect the panels from overheating. In fact, the extra electric energy that might be obtained by a better cooled panel is unlikely to exceed the energy spent to drive the pump needed for cooling. For this reason, the multiplication factor is chosen as a 0/1 boolean condition which activates once the temperature of the panels grows above a certain threshold. To be noted also that UTES states may not be convenient close to the end of the season as it would be counterproductive, for instance, to store heat in the ground at the end of the heating season when this heat is not going to be used due to the milder ambient temperatures, and when soon a colder ground will be preferable. For this reason, the UTES factors in the table include a linear penalty function of time F, defined as the time left until the end of the season divided by the length of the season, so that its value is 1 at the season begin, and 0 at its end.

Finally, in a similar fashion to what done for primary states, a minimum allowable heat transfer rate (ΔT_{sec}) is established below which the system is turned off to save electric energy when too little heat would be transferred by the best secondary state. ΔT_{sec}=1.5 °C is chosen after a set of preliminary simulations.

The general outline of the sources control algorithm proposed is given in Table 5. At first, at each time step, info on the situation of the plant is read, and all the ETPs evaluated (lines 1–9). Then, if the heat pump is on or BF_{src} can be recharged a primary state is selected, otherwise secondary states are taken in consideration. Among primary states, sun or air are chosen if they are best (highest ETP) or if they can cover the target thermal load, *i.e.* $ETP_{src}>\Delta T_{pri}$ (lines 10–16). If this is not the case then ground is exploited, being blended with the second best source in case the target thermal load ΔT_{pri} is exceeded (lines 17–22). In each case, the pump on the sources side is regulated in order to increase the flow rate if the state ETP falls short on the target, and *vice versa*. Among secondary states the best is always chosen, given that it exceeds the minimum threshold ΔT_{sec} (lines 23–30). When a secondary state is selected, the mass flow rate is always set to a predetermined minimum (*i.e.* $\dot{m}$=4000 kg/h) as a high heat transfer rate is not a priority in this case.

2.9. The set of simulations

The performance of the system described in Section 2 is evaluated numerically in terms of primary energy needs for the 5 plant configurations outlined in Section 2.4, the 3 climate areas in Section 2.5, and for

Table 5
Outline of the sources control algorithm.

```
∀ time step
read T_A, T_S, T_G, T_BFsrc, T_BFbld, HP state, time
compute s, F

compute ETP_GA,UTES, ETP_GS,UTES, ETP_AS,PVC, ETP_A,DHC, ETP_S,DHC from Eq. (12)
apply multiplication factor to ETPs of secondary states
ETP_pri = max(ETP_A, ETP_S, ETP_G)
ETP_sec = max(ETP_GA,UTES, ETP_GS,UTES, ETP_AS,PVC, ETP_A,DHC, ETP_S,DHC)
if HP==ON: ΔT_pri = ΔT_max ; else: ΔT_pri = ΔT_min
if (HP==ON) or (ETP_pri ≥ ΔT_pri): # primary states
  P_src = ON
  if ETP_pri ≤ 0: P_src = OFF ; STATE = Idle
  else if (ETP_S == ETP_pri) or ((ETP_S ≥ ETP_A)and(ETP_S ≥ ΔT_pri)):
    STATE = S ; ṁ = 6000 kg/h · max(2/3, min(4/3, ΔT_pri/ETP_S))
  else if (ETP_A == ETP_pri) or ((ETP_A ≥ ETP_S)and(ETP_A ≥ ΔT_pri)):
    STATE = A ; ṁ = 6000 kg/h · max(2/3, min(4/3, ΔT_pri/ETP_A))
  else: # (ETP_G == ETP_pri) and (max(ETP_S, ETP_A) < ΔT_pri)
    if (ETP_S ≥ ETP_A) and (ETP_S ≥ ΔT_min) and (ETP_G > ΔT_pri):
      STATE = GS ; f_G = (ΔT_pri − ETP_S)/(ETP_G − ETP_S) ; ṁ = 6000 kg/h
    else if (ETP_A ≥ ETP_S) and (ETP_A ≥ ΔT_min) and (ETP_G > ΔT_pri):
      STATE = GA ; f_G = (ΔT_pri − ETP_A)/(ETP_G − ETP_A) ; ṁ = 6000 kg/h
    else: STATE = G ; ṁ = 6000 kg/h · max(2/3, min(4/3, ΔT_pri/ETP_G))
else: # secondary states
  P_src = ON ; ṁ = 4000 kg/h
  if ETP_sec ≤ ΔT_sec: P_src = OFF ; STATE = Idle
  else if ETP_GA,UTES == ETP_sec: STATE = GA UTES ; f from Eq. (11)
  else if ETP_GS,UTES == ETP_sec: STATE = GS UTES ; f from Eq. (11)
  else if ETP_AS,PVC == ETP_sec: STATE = AS PVC ; f from Eq. (11)
  else if ETP_A,DHC == ETP_sec: STATE = A DHC ; f from Eq. (11)
  else: STATE = S DHC ; f from Eq. (11) # ETP_S,DHC == ETP_sec
```

Table 6
Resume of the simulations performed.

Parameter	Possible values
Thermal Transmittance [W/m^{2}K]	0.25 ; 0.35 ; 0.50 ; 0.70 ; 0.70 brick walls & 1.10 glazed windows
Climate Area	Ferrara ; Lisbon ; Dublin
Plant Configuration	CC ; MS-PC; MS-XC; SS-PC; SS-XC

5 different values of the wall thermal transmittance U (see Section 2.1) for a total of 5×3×5=75 simulations. Table 6 resumes the possible values of the three parameters, where all their permutations are evaluated in TRNSYS.

The simulations are performed starting from the beginning of the heating season and are run throughout the year with time steps of 5 minutes. The components are initialised, in terms of average thermal field, after a preliminary 1-year run. Although computationally expensive, the preliminary run is important for the correct thermal initialisation of components characterised by large thermal inertia, such as the ground source. At each time step, results in terms of temperature, and energy and mass transfer at each type are saved to file for the successive post-processing. The default TRNSYS solver setup is adopted which includes a second order Runge–Kutta scheme for differential equations (named modified Euler method), and the use of the successive substitution method solving the equations of each type in succession and iterating up to convergence within each time step. The convergence tolerance is set to 10^{-4}.

To be noted that the building presented in Section 2.1 is characterised by very large glazed surface area that might be kind of common in commercial buildings, but would be rather unusual in domestic ones. To evaluate the thermal behaviour of the building in different scenarios the glazed windows are at first substituted by brick walls and the walls thermal transmittance changed from 0.25 to 0.70 W/m^{2}K as in Table 6. In the last step, a simulation is added where the glazed windows are modelled as in Section 2.1 and the brick walls thermal transmittance is kept at U=0.70 W/m^{2}K.

It is reminded that the current analysis only addresses the heating and cooling needs of the building and does not include the modelling of any additional electrical equipment, such as lighting for instance, in terms of electric consumption and thermal gain, nor the energy consumption ascribable to hot sanitary water.

3. Results

The main results of the simulations are discussed in the following in terms of thermal needs of the building, electric consumption of the RES, sources exploitation, and primary energy needs.

At first, due to the large number of simulations, a more detailed analysis of the most thermally loaded scenario is given.

3.1. The Ferrara glazed windows building

The most thermally loaded scenario for what concerns both the building needs and the sources exploitation is found to be the Ferrara building with glazed windows, which is also the real scenario where the RES proposed is to be installed. As a reference configuration the multi-source planned one is chosen, similar results can be found for the other configurations tested.

Let us focus at first on the building thermal needs. These do not depend on the configuration chosen (the building is always the same) if not, to a lesser extent, for the case of the current configuration where the floor is not an active heating/cooling surface (the CC features no radiant floor) but an extra thermal dissipation surface. Fig. 6 shows the room energy balance along the year in terms of thermal energy delivered by the radiant floor and the fan coil through the AHU, dispersed to the ambient through the walls (this term also includes solar radiation gains), and the thermal loss to be ascribed to the air change rate. The histogram in the figure and those that will follow subdivide the year in 24 periods of 365 hours (≈15 days) each. To be noted how a large share of the building thermal needs is covered by the radiant floor. The role of the AHU is marginal except for the months of July and August due to the high humidity of summers in Ferrara. This is confirmed by the high thermal energy cost of fresh air

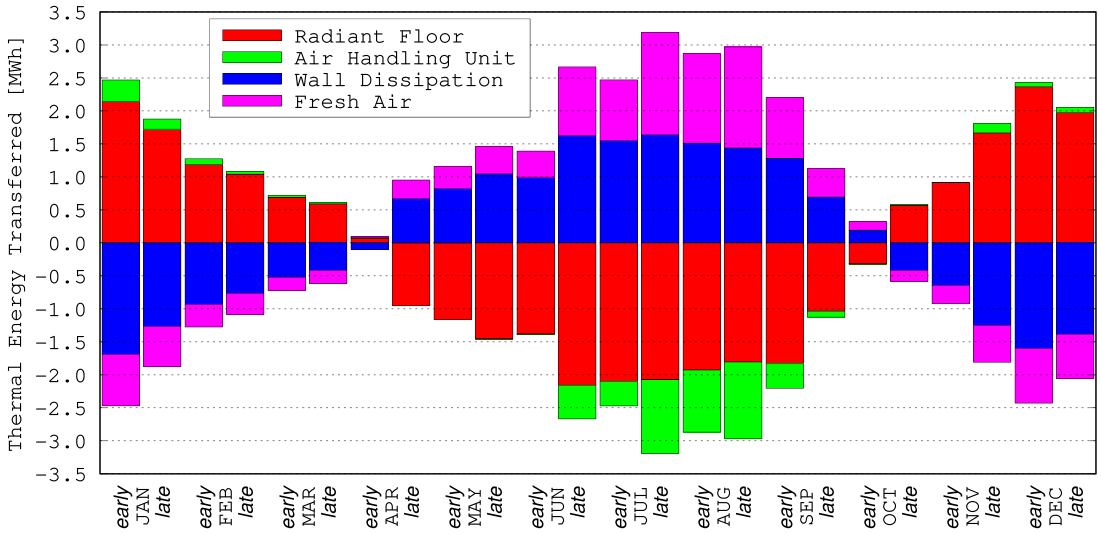

(a) Thermal energy delivered to and removed from the building, and dissipated through the walls

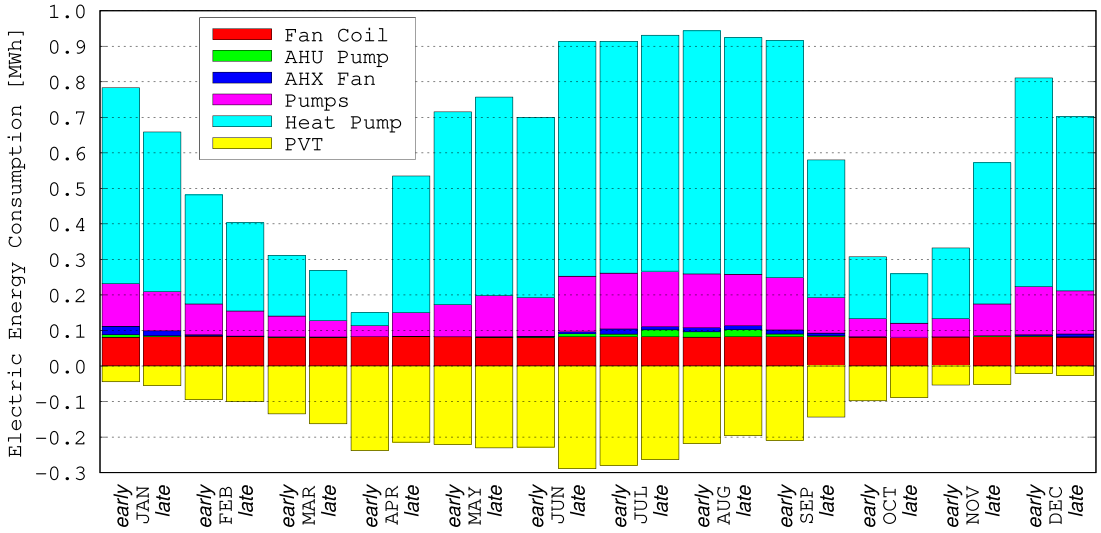

(b) System electric energy consumption. On the negative half plane the PVT electric energy production is reported

Fig. 6. Ferrara glazed windows building with multi-source planned RES configuration: main numerical results over the year.

conditioning in summer. Solar radiation through the glazed windows contributes in keeping the balance of the wall dissipation relatively low in winter (when the room to ambient temperature difference is higher on average), while the opposite occurs in summer.

Fig. 6b shows the RES electric energy consumption in a similar fashion. The consumption of the fan coil is mostly connected to the constant ventilation in order to meet the required air change rate, if not for rare occasions in which the fan coil may also be switched on at night to support the radiant floor operation. The ventilation is active 12 hours a day and absorbs 450 W, summing up to ≈80 kWh over a fortnight. Consumption of the AHU pump and the AHX fan are negligible being these devices rarely employed, whereas by far the largest share of electric energy is needed to drive the heat pump. The electric production of the photovoltaic panels is reported on the negative half plane of the plot.

Fig. 6c reports the exploitation of the sources in terms of thermal energy drawn from them. Here the largest share is delivered by GHX, with the PVT providing a good support almost all year round. AHX is much less exploited due to its lesser heat transfer efficiency and its higher electric energy cost due to the additional fan involved. The thermal load on the sources is higher during summer despite the building energy demand being similar between the heating and cooling seasons due to the inversion of the heat pump operation mode. To be noted how the exploitation of the ground drops close to the end of the seasons.

Fig. 6d shows the different system states in terms of their use over time. While the system remains idle for approximately 34% of time during the cooling season and 61% in the heating season, the largest share of active time is covered by primary states, with a leading role played by sun (S state) followed by ground (G state) while air (A state) is rather seldomly exploited. The larger amount of thermal energy provided by the ground together with the lesser usage time compared to sun denotes a much larger thermal power capacity of the ground heat exchanger mostly due to the larger heat transfer area available. GA and GS states are almost never used due to the high $\Delta T_{\max}$ resulted from the control algorithm calibration. The same occurs to the air-based secondary states for the reasons outlined above that translate into low values of ε_A and of the multiplication factor in the control algorithm.

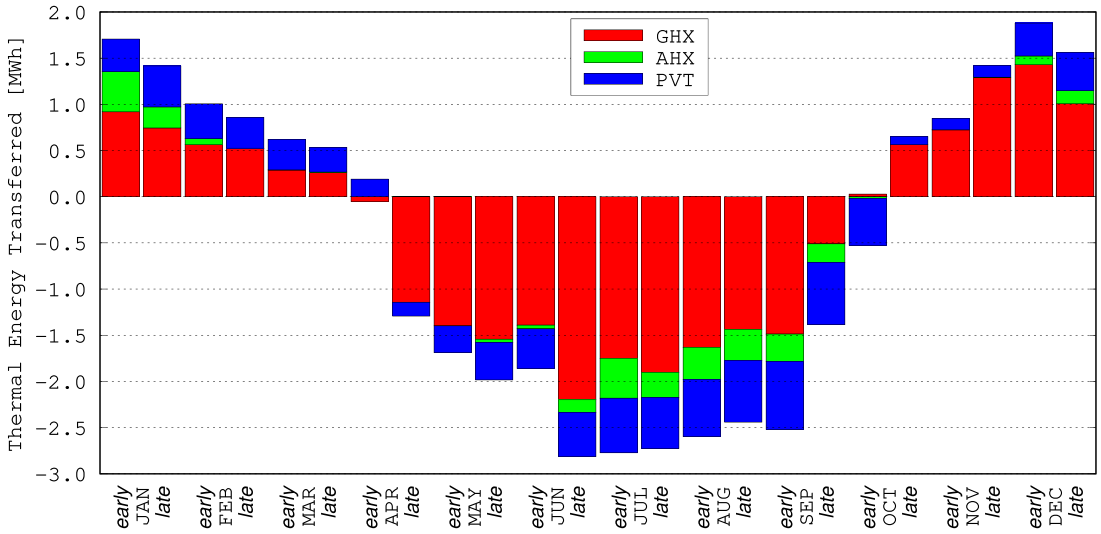

(c) Thermal energy drawn from the sources. Positive numbers stand for heat, negative for cool drawn from the sources

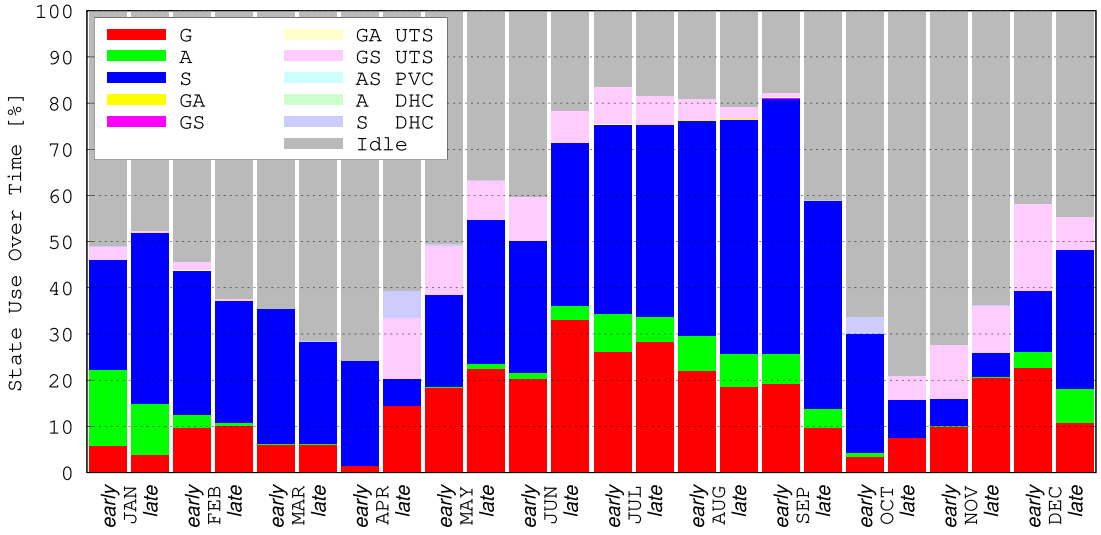

(d) Percentage of use over time of the different system states

Fig. 6. (*continued*).

Secondary states are exploited for only 6% of time year round, whereas the choice falls almost uniquely on GS UTES, with the exception of S DHC that can be found very early and very late during the cooling season. The large PVT usage time is concentrated during the day in the heating season due to the high temperature that the cells can reach on clear days, and at night or early morning in the cooling season where the temperature of the cells can drop below that of air.

Tables 7 and 8 resume the main results of Fig. 6 for the heating and the cooling seasons in terms of thermal energy transfer, electric energy consumption, and usage time for each device and state of the system. In Table 7 the usage time for the three sources is to be intended as the time fraction spent working in direct mode, *i.e.* the ground secondary states where the GHX operates in inverse mode are not accounted for. Similarly, the usage time for the photovoltaic panels in terms of electric energy is assumed to be the daytime, *i.e.* the time over which the electric energy production is not null. With reference to Table 8 is to be noted that some possible system states are actually never chosen and are omitted from the list, these are: GA UTES, AS PVC, and A DHC.

3.2. Building thermal needs

The building thermal needs in terms of heating and cooling are covered by the radiant floor and the fan coil, either through the AHU or the heat pump depending on the system configuration. Of course, the amount of thermal energy required depends on the building, on the environment (*i.e.* the climate area), and on the target setpoint temperature chosen, while it does not depend on the mean by which the required thermal energy is provided. As such, from the numerical simulations performed, the different configurations tested show the same thermal needs, within a margin of error of ±2%, for a given climate area and wall thermal transmittance value.

Fig. 7 shows the heating and cooling needs of the snack bar building for the different climate areas and wall U values tested. The values reported in each bar are the average resulting from single-source and multi-source configurations. The figure also distinguishes between the thermal energy provided by the radiant floor in thicker colours, and by the fan coil in lighter colours.

The role of the fan coil is always very marginal, if not for the cooling season in Ferrara due to high humidity. For the brick walls cases of

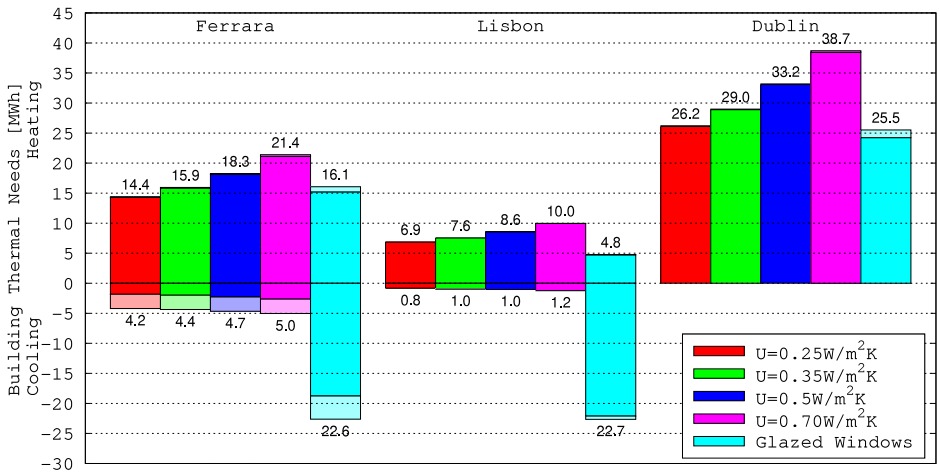

Fig. 7. Building thermal needs for the different climate areas and U values tested. Thicker colours represent the portion of heat delivered by the radiant floor, lighter colours the portion delivered by the fan coil. Heating needs are drawn in the positive half plane, cooling needs in the negative half plane.

Table 7
Ferrara glazed windows building with multi-source planned RES configuration: components heat transfer and electric energy consumption over the seasons. Positive thermal energy stand for heat transferred to the building or drawn from the sources, and *vice versa*. Negative electric energy consumptions stand for the PVT production.

		Energy [MWh]		Usage Time [%]	
		Heating season	Cooling season	Heating season	Cooling season
Thermal Energy	Radiant Floor	14.95	−18.20	16.8	24.1
	AHU	0.96	−4.58	1.7	5.8
	Walls	−10.98	13.48	100.0	100.0
	Fresh Air	−4.92	9.30	50.0	50.2
	GHX	8.20	−16.56	9.6	19.7
	AHX	1.08	−2.07	3.5	3.8
	PVT	3.37	−5.95	26.2	42.3
Electric Energy	Fan Coil	0.98	0.99	50.0	50.2
	AHU Pump	0.02	0.08	1.7	5.8
	AHX Fan	0.08	0.08	3.5	3.8
	Sources Pump	0.67	1.10	39.3	65.9
	Building Pump	0.14	0.19	16.8	24.1
	Recirculation Pumps	0.15	0.15	15.4	15.5
	Heat Pump	3.72	6.55	15.4	15.5
	Photovoltaic Panels	−1.07	−2.59	42.0	55.8

Table 8
Ferrara glazed windows building with multi-source planned RES configuration: system states percentage of use over time.

State	G	A	S	GA	GS	GS UTES	S DHC	Idle
Heating Season	9.6%	3.5%	21.3%	0.0%	0.0%	4.9%	0.0%	60.7%
Cooling Season	19.7%	3.8%	35.6%	<0.1%	<0.1%	5.9%	0.8%	34.1%

course the thermal needs grow with the wall thermal transmittance. Moderate cooling needs are found overall, while heating needs in Dublin are almost double than in Ferrara and fourfold with respect to Lisbon. Things change noticeably for the glazed windows case due to the relevance of solar thermal radiation over such large south facing glazed surface area. In this case the heating needs are reduced up to being halved in Lisbon, while the cooling needs are increased up to 18 times still in Lisbon where solar radiation is stronger.

3.3. Electric energy consumption

Electric energy consumption is given by the various system devices such as pumps, fans, and the heat pump. Multi-source configurations also feature the photovoltaic panels producing a certain amount of electric energy. The consumption resulting from all the 75 simulations performed is resumed in Fig. 8. The figure distinguishes between the contributions of the heat pump in thicker colours, the other devices in lighter colours, and the photovoltaic panels on the negative half plane. It further distinguishes between the electric consumption during heating and cooling seasons. The bars are in groups of five, representing the system configurations tested. From left to right the five U values are found for the three climate areas evaluated.

The current configuration is characterised by very low electric energy consumptions as the thermal energy is not provided by a heat pump. To be noted how the consumption of extended configurations is always larger compared to the corresponding planned configurations because of the extra thermal load on the heat pump given by the fan coil. To be noted also that multi-source configurations always show a lesser electric energy consumption compared to their corresponding single-source versions denoting an increased system efficiency granted by the availability of multiple sources to choose from. Of course PVT electric energy production changes with the location, but not with the multi-source configuration and the system thermal load, meaning that different panels cooling after different thermal exploitations of the PVT only have a marginal impact on the panels electric production.

3.4. Sources exploitation

Multi-source configurations can exploit ground, air, and sun as renewable thermal sources, whereas their single-source counterparts exploit only air. Current configurations are omitted from this analysis as they do not rely on renewable energy sources.

Fig. 9 shows the thermal sources exploitation from all the 60 simulations based on renewable energy. The figure distinguishes between the three sources with different colours, and between the sources exploitation during the heating season in the positive half plane, and the cooling season in the negative half plane. The bars are in group of four, representing the single and the multi-source system configurations tested. From left to right the five U values are found for the three climate areas evaluated.

In a similar fashion to what discussed for electric energy consumption, extended configurations show a larger overall sources exploitation compared to their planned counterparts, at least for the cases where the heating/cooling role of fan coil is not null, otherwise the two configurations essentially behave the same. Similarly, multi-source configurations show a lesser sources exploitation compared to their single-source versions. Concerning multi-source configurations, it can be noted that the role of GHX in terms of thermal energy provided is always particularly relevant. Depending on the configuration, the U value, and the season, the GHX provides a share between 57% and 85% of the total renewable energy in Ferrara, and between 68% and 79% in

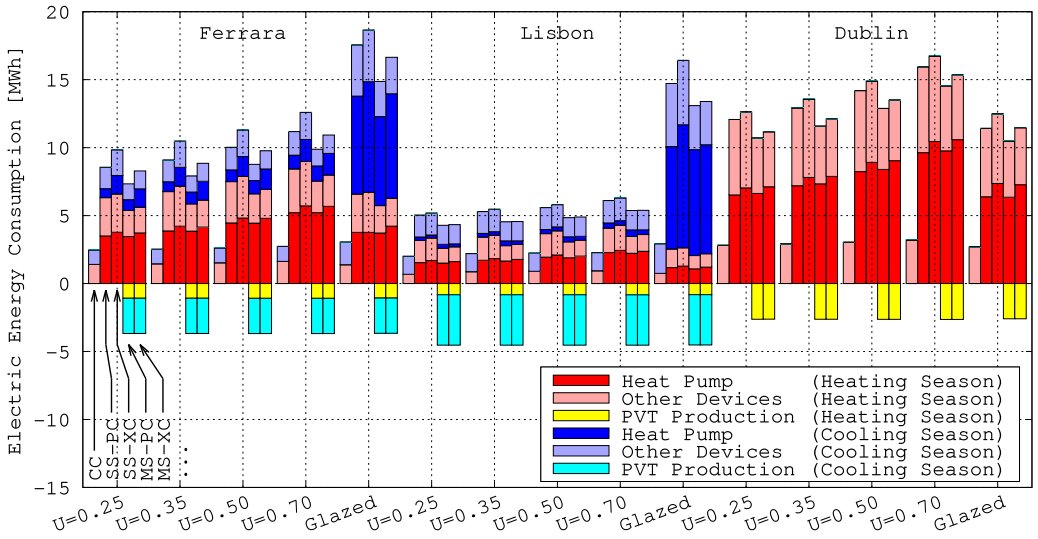

Fig. 8. System electric energy consumption for the different climate areas, U values, and system configurations tested. On the positive half plane thicker colours represent the heat pump consumption in heating and cooling modes, lighter colours the consumption of all the other devices. On the negative half plane the PVT electric production is reported.

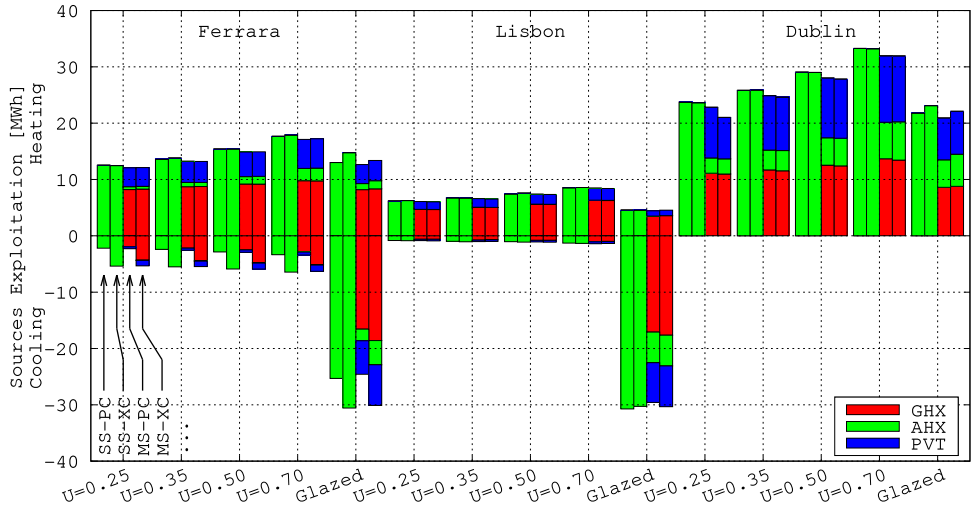

Fig. 9. Sources exploitation in terms of thermal energy for the different climate areas, U values, and system configurations tested. Heating demands are drawn in the positive half plane, cooling demands in the negative half plane.

Lisbon, these shares being slightly reduced for the cooling season glazed window cases due to the excessive thermal load on the source that tends to deplete it rapidly. A lesser GHX exploitation, between 40% and 52%, is found in Dublin where the exploitation of ground always occurs in one direction, except for the secondary role played by UTES, as there is no cooling season. This prevents the source from being recharged by the alternate use made through the seasons: a depleted ground for the heating season in fact becomes an optimal source for the cooling season and *vice versa*. This leaves margins to PVT exploitation, which in Dublin is between 34% and 39%, while it remains between 15% and 32% in Ferrara and Lisbon. AHX exploitation is less relevant, being nearly zero in most cases, and reaching up to 18% during the cooling season in Ferrara and Lisbon glazed windows cases. Air exploitation in Dublin settles between 12% and 26%.

3.5. Primary energy

The required thermal energy is provided to the building by the heat pump driven multi-source system and/or by the AHU.

In order to evaluate the performance of a configuration in terms of primary energy needs, the AHU heat transfer must be accounted, together with the electrical consumption of all the system devices, namely: AHU pump, fan coil, AHX fan, heat pump, circulation pumps, pumps on the sources and on the building side. No heat transfer to and from the sources is to be included, being the sources renewable. Besides, energy conversion efficiency factors η are needed to quantify the relative primary energy cost of heating and cooling from the AHU, and of electric energy. For what concerns the latter, a thermal to electric conversion efficiency η_{el}=0.45 at the power plant is assumed. About the thermal energy cost of the AHU operation much depends on the mean by which the energy is obtained. Here it is hypothesised that heating is obtained from a rather common high efficiency condensing boiler having a thermal efficiency η_{ht}=0.95, while cooling from an air conditioning unit having COP of 2.5 (η_{cl}=COPη_{el}=1.125).

The primary energy consumption E_p can then be evaluated as

$$E_p = \frac{Q_{ht}}{\eta_{ht}} + \frac{Q_{cl}}{\eta_{cl}} + \frac{E_{el}}{\eta_{el}} \tag{13}$$

where Q_{ht} and Q_{cl} refer to the thermal energy from the AHU, and E_{el} to the global electric energy consumption of the system. The first two terms on the right-hand side of the equation are null in the extended configuration which features no AHU.

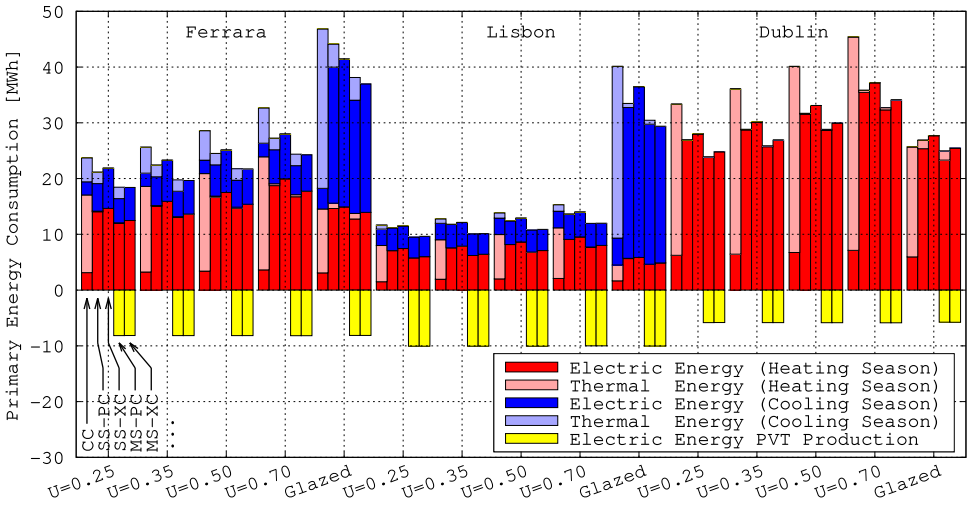

Fig. 10. Primary energy needs for the different climate areas, U values, and system configurations tested. On the positive half plane thicker colours represent the portion of primary energy due to electric energy (third term on the right-hand side of Eq. (13)), lighter colours the portion due to thermal energy (first and second term of Eq. (13)). On the negative half plane the primary energy savings due to the PVT electric production are reported.

Table 9
Reduction of the building primary energy needs of the multi-source RES with respect to the corresponding current and single-source configurations for different climate areas and U values.

	U [W/m^{2}K]	0.25	0.35	0.50	0.70	Glazed windows
Ferrara	MS to CC	22.4%	23.1%	24.0%	25.6%	19.8%
	MS to SS	14.3%	13.7%	12.4%	11.9%	12.2%
Lisbon	MS to CC	17.9%	20.8%	21.9%	21.9%	25.4%
	MS to SS	15.6%	15.4%	14.4%	13.3%	14.5%
Dublin	MS to CC	27.0%	26.9%	26.7%	26.5%	1.9%
	MS to SS	11.4%	10.6%	9.3%	8.5%	7.6%

Fig. 10 shows the primary energy needs, computed from Eq. (13), resulting from all the 75 simulations performed. The figure distinguishes between heating season in thicker colours, and cooling season in lighter colours, and between the contributions of electric energy (third term on the right-hand side of Eq. (13)), and of thermal energy (first two terms on the right-hand side of Eq. (13)). On the negative half plane the primary energy savings obtained thanks to the photovoltaic panels are also reported. The bars are in groups of five, representing the system configurations tested. From left to right the five U values are found for the three climate areas evaluated.

To be noted that current configurations results always the worst in terms of primary energy needs, whereas multi-source configurations always overperform the others even without taking into account the photovoltaic panels electric energy production. Assuming that the plant is able to fully exploit the electric energy produced by the panels, multi-source configurations can reach a nearly zero energy building condition in Lisbon where the photovoltaic production is high, and the thermal load on the building low, given that the building is well thermally insulated.

For a fairer comparison between the different configurations, the PVT production is excluded from the following calculations. In this way, the effective primary energy reductions directly ascribable to the more efficient handling of thermal energy in the multi-source RES can be better quantified. Rather than the comparison between multi-source and current configurations, as the latter are not particularly efficient *per se*, it is more interesting to compare multi-source configurations with their single-source counterparts in order to evaluate the advantage brought by the proposed RES with respect to a more common state-of-the-art single-source solution. Table 9 resumes these comparisons in terms of percent primary energy needs reduction. Consistent reductions between 12% and 16% are seen in Ferrara and Lisbon for multi-source solutions with respect to the single-source. The advantage is slightly thinning for the most thermally loaded cases where the ground source suffers from over-exploitation. The gain is less evident in Dublin where it settles between 8% and 11%. This is due to the lesser exploitation of the GHX due to the ground source depletion, and the larger exploitation of the AHX which is more costly in terms of electric energy. The advantage with respect to the current configuration is higher and settles between 18% and 27%. A very peculiar case is given by the glazed windows building in Dublin. There, the current configuration is found to overperform the single-source, while the multi-source behaves barely better (<2% gain). Compared to the other Dublin cases, in the glazed window building the thermal load on the sources is largely shifted from summer, where the load is almost zero thanks to the solar radiation gain, to winter, where very high thermal loads are found. In case the only available source is cold air, the heat pump performance suffers and the electric energy consumption is increased. Things turn out slightly better for the multi-source case which yet pays the penalty of a too large AHX exploitation in winter, and a relevant GS UTES exploitation in summer which despite the high electric energy cost, is not able to store as much thermal energy in the ground as desired. Such a behaviour could be improved by further tuning the system control algorithm, and highlights the relevance of climate area dependent controls for an optimal system performance.

4. Conclusions

A numerical analysis of a multi-source renewable energy system for building air conditioning has been presented. The energy system proposed can exploit air, sun, and shallow ground as thermal sources through proper heat exchangers. A heat pump supplies the required thermal energy to the building by feeding a PCM-integrated radiant floor and a fan coil at need. The presence of multiple sources implies the definition of a detailed system control algorithm able to decide the best sources to be exploited at any time thus providing the required thermal energy to the heat pump, and eventually storing the thermal energy in excess when the heat pump is idle. A novel control algorithm based on the prediction of the thermal power that could be drawn from the sources at each time for given system temperature boundary conditions was presented and discussed in detail. The renewable energy system, together with the control algorithm proposed, was numerically tested on a sample building consisting of a snack bar on the University of Ferrara campus. The building was investigated for different renewable energy

system configurations, walls thermal transmittances, and geographic locations to assess the reduction in terms of primary energy needs that could be achieved in comparison to an analogous single-source state-of-the-art system under different scenarios.

Shallow ground has been demonstrated to be the most prominent thermal source for these kinds of applications, providing a thermal energy share of ≈70% in continental and mediterranean climates on average, the limit being its possible thermal depletion if over-exploited. This calls for larger geothermal installation areas where possible, and more careful exploitation of the ground source by adopting a system control able to preserve it from excessive exploitation.

In line with this, the crucial role of the control algorithm on the thermal performance of the whole system has been demonstrated, highlighting how an optimal control should be tuned on the system size, the thermal load, and the climate area. The thermal power-based control methodology proposed has been demonstrated to be effective in preserving the ground source from over-exploitation despite the relatively small geothermal field installed in the sample building.

The proposed system showed reductions in terms of primary energy needs between 12% and 16% compared to an analogous single-source air-based system, and up to 26% compared to an ordinary condensing boiler and domestic air conditioner system in continental and mediterranean climates. In colder climates, where for instance the imbalance between the heating and the cooling needs throughout the year is apparent, the gain is thinned at 8% to 12% compared to the chosen single-source benchmark system. More consistent reductions are expected with the installation of larger geothermal fields. The multi-sources system proposed, in fact, is found to rely primarily on the shallow ground source. Even though such a source is thermally recharged by the ambient through the ground surface, this process occurs slowly over the seasons due to the large thermal capacity of the ground. This is the main reason that makes shallow ground advantageous being its temperature essentially out of phase with the ambient. Yet, it also implies that shallow ground exploitation works best in an environment where it can be used alternatively for heating and cooling purposes throughout the year, thus limiting its temperature deviation from the undisturbed soil condition that would make the source less attractive.

CRediT authorship contribution statement

Marco Cavazzuti: Conceptualization, Methodology, Software, Validation, Formal analysis, Investigation, Data curation, Writing – original draft, Writing – review & editing, Visualization. **Michele Bottarelli:** Resources, Supervision, Project administration, Funding acquisition.

Declaration of competing interest

The authors declare the following financial interests/personal relationships which may be considered as potential competing interests: Michele Botarelli reports financial support was provided by European Commission.

Data availability

Data will be made available on request.

Acknowledgements

This work was supported by the European Union's Horizon 2020 research and innovation programme under grant agreement No 815271.

References

[1] Pérez-Lombard H, Ortiz J, Pout C. A review on buildings energy consumption information. Energ Build 2008;40(3):394–8.
[2] Sinsel S, Riemke R, Hoffmann V. Challenges and solution technologies for the integration of variable renewable energy sources – A review. Renew Energ 2020;145:2271–85.
[3] Yang M, Li Z, Reese M, Reid O, Kim D, Siol S, et al. Perovskite ink with wide processing window for scalable high-efficiency solar cells. Nat Energ 2017;2(5):17038.
[4] Eperon G, Hörantner M, Snaith H. Metal halide perovskite tandem and multiple-junction photovoltaics. Nat Rev Chem 2017;1(12):0095.
[5] Nozik A, Beard M, Luther J, Law M, Ellingson R, Johnson J. Semiconductor quantum dots and quantum dot arrays and applications of multiple exciton generation to third-generation photovoltaic solar cells. Chem Rev 2010;110(11):6873–90.
[6] Wu J, Mangham S, Reddy V, Manasreh M, Weaver B. Surface plasmon enhanced intermediate band based quantum dots solar cell. Sol Energ Mat Sol C 2012;102:44–9.
[7] Bernardoni P, Mangherini G, Gjestila M, Andreoli A, Vincenzi D. Performance optimization of luminescent solar concentrators under several shading conditions. Energies 2021;14(4):816.
[8] Ahmed H, McCormack S, Doran J. Plasmonic luminescent down shifting layers for the enhancement of CdTe mini-modules performance. Sol Energy 2017;141:242–8.
[9] Alexandre M, Chapa M, Haque S, Mendes M, Águas H, Fortunato E, et al. Optimum luminescent down-shifting properties for high efficiency and stable perovskite solar cells. ACS Appl Energ Mater 2019;2(4):2930–8.
[10] Tian M, Su Y, Zheng H, Pei G, Li G, Riffat S. A review on the recent research progress in the Compound Parabolic Concentrator (CPC) for solar energy applications. Renew Sust Energ Rev 2018;82(1):1272–96.
[11] Sethi A, Chandra S, Ahmed H, McCormack S. Broadband plasmonic coupling and enhanced power conversion efficiency in luminescent solar concentrator. Sol Energ Mat Sol C 2019;203:110150.
[12] Chen S, Cai W, Witte F, Wang X, Wang F, Kolditz O, Shao H. Long-term thermal imbalance in large borehole heat exchangers array – A numerical study based on the Leicester project. Energ Build 2021;231:110518.
[13] Cimmino M, Eslami-Nejad P. A simulation model for solar assisted shallow ground heat exchangers in series arrangement. Energ Build 2017;157:227–46.
[14] Bottarelli M, Bortoloni M, Su Y, Yousif C, Aydın A, Georgiev A. Numerical analysis of a novel ground heat exchanger coupled with phase change materials. Appl Therm Eng 2015;88:369–75.
[15] Gabrielli L, Bottarelli M. Financial and economic analysis for ground-coupled heat pumps using shallow ground heat exchangers. Sustain Cities Soc 2016;20:71–80.
[16] Najib A, Zarrella A, Narayanan V, Bourne R, Harrington C. Techno-economic parametric analysis of large diameter shallow ground heat exchanger in California climates. Energ Buildings 2020;228:110444.
[17] Javadi H, Ajarostaghi S, Rosen M, Pourfallah M. Performance of ground heat exchangers: A comprehensive review of recent advances. Energy 2019;178:207–33.
[18] Schiel K, Baume O, Caruso G, Leopold U. GIS-based modelling of shallow geothermal energy potential for CO_2 emission mitigation in urban areas. Renew Energ 2016;86:1023–36.
[19] Haehnlein S, Bayer P, Blum P. International legal status of the use of shallow geothermal energy. Renew Sust Energ Rev 2010;14(9):2611–25.
[20] Tsagarakis K, Efthymiou L, Michopoulos A, Mavragani A, Andelković A, Antolini F, et al. A review of the legal framework in shallow geothermal energy in selected European countries: Need for guidelines. Renew Energ 2020;147(2):2556–71.
[21] Algieri A, Morrone P, Perrone D, Bova S, Castiglione T. Analysis of multi-source energy system for small-scale domestic applications. Integration of biodiesel, solar and wind energy. Energ Rep 2020;6(1):652–9.
[22] Palomba V, Borri E, Charalampidis A, Frazzica A, Cabeza L, Karellas S. Implementation of a solar-biomass system for multi-family houses: towards 100% renewable energy utilization. Renew Energ 2020;166:190–209.
[23] Emmi G, Zarrella A, Carli MD. A heat pump coupled with photovoltaic thermal hybrid solar collectors: a case study of a multi-source energy system. Energ Convers Manage 2017;151:386–99.
[24] Samy M, Barakat S, Ramadan H. Techno-economic analysis for rustic electrification in Egypt using multi-source renewable energy based on PV/wind/FC. Int J Hydrogen Energ 2020;45:11471–83.
[25] Zhang W, Maleki A, Nazari M. Optimal operation of a hydrogen station using multi-source renewable energy (solar/wind) by a new approach. J Energ Stor 2022;53:104983.
[26] Sayed E, Wilberforce T, Elsaid K, Rabaia M, Abdelkareem M, Chae K-Y, et al. A critical review on environmental impacts of renewable energy systems and mitigation strategies: Wind, hydro, biomass and geothermal. Sci Total Environ 2021;766:144505.
[27] Catalina T, Virgone J, Blanco E. Multi-source energy systems analysis using a multi-criteria decision aid methodology. Renew Energ 2011;36(8):2245–52.

[28] Park S-H, Jang Y-S, Kim E-J. Multi-objective optimization for sizing multi-source renewable energy systems in the community center of a residential apartment complex. Energ Convers Manage 2021;244:114446.
[29] Deshmukh M, Deshmukh S. Modeling of hybrid renewable energy systems. Renew Sust Energ Rev 2008;12(1):235–49.
[30] Lian J, Zhang Y, Ma C, Yang Y, Chaima E. A review on recent sizing methodologies of hybrid renewable energy systems. Energ Convers Manage 2019;199:112027.
[31] Olabi A, Mahmoud M, Soudan B, Wilberforce T, Ramadan M. Geothermal based hybrid energy systems, toward eco-friendly energy approaches. Renew Energ 2020;147(1):2003–12.
[32] Stadler P, Ashouri A, Maréchal F. Model-based optimization of distributed and renewable energy systems in buildings. Energ Build 2016;120:103–13.
[33] Suganthi L, Iniyan S, Samuel A. Applications of fuzzy logic in renewable energy systems – a review. Renew Sust Energ Rev 2015;48:585–607.
[34] Amrouche SO, Rekioua D, Rekioua T, Bacha S. Overview of energy storage in renewable energy systems. Int J Hydrogen Energ 2016;41(45):20914–27.
[35] Koukou M, Vrachopoulos M, Tachos N, Dogkas G, Lymperis K, Stathopoulos V. Experimental and computational investigation of a latent heat energy storage system with a staggered heat exchanger for various phase change materials. Therm Sci Eng Prog 2018;7:87–98.
[36] Jegadheeswaran S, Pohekar S. Performance enhancement in latent heat thermal storage system: A review. Renew Sust Energ Rev 2016;13(9):2225–44.
[37] Fleming E, Wen S, Shi L, da Silva A. Experimental and theoretical analysis of an aluminum foam enhanced phase change thermal storage unit. Int J Heat Mass Tran 2015;82:273–81.
[38] Qi G-Q, Liang C-L, Bao R-Y, Liu Z-Y, Yang W, Xie B-H, et al. Polyethylene glycol based shape-stabilized phase change material for thermal energy storage with ultra-low content of graphene oxide. Sol Energ Mat Sol C 2014;123:171–7.
[39] Cabeza L, Ibánez M, Solé C, Roca J, Nogués M. Experimentation with a water tank including a PCM module. Sol Energ Mat Sol C 2006;90(9):1273–82.
[40] Ansuini R, Larghetti R, Giretti A, Lemma M. Radiant floors integrated with PCM for indoor temperature control. Energ Build 2011;43(11):3019–26.
[41] Lakhdari Y, Chikh S, Campo A. Analysis of the thermal response of a dual phase change material embedded in a multi-layered building envelope. Appl Therm Eng 2020;179:115502.
[42] Triano-Juárez J, Macias-Melo E, Hernández-Pérez I, Aguilar-Castro K, Xamán J. Thermal behavior of a phase change material in a building roof with and without reflective coating in a warm humid zone. J Build Eng 2020;32:101648.
[43] Mahdaoui M, Hamdaoui S, Msaad AA, Kousksou T, Rhafiki TE, Jamil A, et al. Building bricks with phase change material (PCM): Thermal performances. Constr Build Mater 2021;269:121315.
[44] Liu B, Zhang X, Ji J. Review on solar collector systems integrated with phase-change material thermal storage technology and their residential applications. Int J Energ Res 2021;45(6):8347–69.
[45] Akbari H, Browne M, Ortega A, Huang M, Hewitt N, Norton B, et al. Efficient energy storage technologies for photovoltaic systems. Sol Energy 2019;192:144–68.
[46] Sohani A, Dehnavi A, Sayyaadi H, Hoseinzadeh S, Goodarzi E, Garcia DA, et al. The real-time dynamic multi-objective optimization of a Building Integrated Photovoltaic Thermal (BIPV/T) system enhanced by phase change materials. J Energ Stor 2022;46:103777.
[47] Bottarelli M, Bortoloni M, Su Y. Heat transfer analysis of underground thermal energy storage in shallow trenches filled with encapsulated phase change materials. Appl Therm Eng 2015;90:1044–51.
[48] da Cunha J, Eames P. Thermal energy storage for low and medium temperature applications using phase change materials – A review. Appl Energ 2016;177:227–38.
[49] Faraj K, Khaled M, Faraj J, Hachem F, Castelain C. Phase change material thermal energy storage systems for cooling applications in buildings: A review. Renew Sust Energ Rev 2020;119:109579.
[50] Jouhara H, Zabnieńska-Góra A, Khordehgah N, Ahmad D, Lipinski T. Latent thermal energy storage technologies and applications: A review. Int J Thermofluids 2020;5–6:100039.
[51] Ciriello V, Bottarelli M, Federico VD, Tartakovsky D. Temperature fields induced by geothermal devices. Energy 2015;93:1896–903.